ELSEVIER

0955-2219(95)00002-X

Journal of the European Ceramic Society 15 (1995) 759–768

0955-2219/95/$9.50

Compaction and Sintering Behaviour of Zirconia Powders

M. Taha,[a] J. Paletto,[a] Y. Jorand,[a] G. Fantozzi,[a]
A. Samdi,[b]* M. Jebrouni[b]** & B. Durand[c]

[a]G.E.M.P.P.M., CNRS URA 341, I.N.S.A. de Lyon, F 69621 Villeurbanne, France
[b]Laboratoire de Chimie Minérale III, URA CNRS 116, I.S.I.D.T. Université Claude Bernaud, Lyon I, 69622 Villeurbanne Cedex, France
[c]Laboratoire des Matériaux Minéraux, URA 428, ENSCMu, 68093 Mulhouse Cedex, France

(Received 23 May 1994; revised version received 22 October 1994; accepted 12 December 1994)

Abstract

Four kinds of zirconia powders are prepared in different ways. Their compaction and sintering behaviour are studied extensively. During compaction, the agglomerates or granules present in the powder are broken and/or undergo plastic deformation. The behaviour depends essentially on the strength of links between the particles.

The sol-gel powders are more sensitive to the formation of hard inter-particle links during the synthesis process. So careful control is needed in order to avoid the formation of aggregates, because they favour the presence of large pores which lead to differential sintering and grain coarsening.

In other cases the sintering can also be inhibited by the presence of residual impurities. A powder which has rod-like shaped agglomerates is sintered to regular microstructure.

Introduction

Uniaxial dry pressing is the most common forming process used to obtain green ceramic bodies in technology today. This process is of great interest technologically because it conditions the quality of fired ceramic bodies, which are influenced by the characteristics of the starting powders.

The presence of hard agglomerates in the powders was reported to be the main source of microstructural inhomogeneities in green ceramic bodies.[1–3] They are formed during the synthesis of the powder.

The purpose of this work was to compare the compaction and sintering behaviours of zirconia powder prepared by several laboratories with a commercial zirconia powder P1.† The following synthesis methods were used:

- Sol–gel process[4] was used for the first batches of powder, (P2, P3).
- Drying of amorphous gelatinous precipitates obtained by hydrolysis of solutions containing both zirconium and yttrium acetates[5] for the second batch, (P4).
- Reaction of both zirconyl and yttrium chlorides in molten salt[6] for the final batch, (P5).

The comparison was likely to give some information about the respective processes involved and could help to optimize the physico-chemical parameters in order to produce high quality zirconia powders.

Experimental procedure

The synthesis processes used to prepare the five batches of zirconia are summarized in Fig. 1.

The powder, P1, was prepared by hydrolysis of a solution containing zirconia and yttria chlorides. It was obtained from calcinated gel. It was then milled and atomized.

The powder, P2, was prepared from a solution containing both zirconia and yttria salts. Ammonia was used as the neutralising agent. The gel was first washed using water, then dried using hexanol. The obtained spheroidal xerogel particles were finally calcinated at 700°C.

The powder, P3, was obtained by coprecipitation of gel. This was later prepared from zirconia and yttria chlorides. The gel was washed three times using water, then three times using pure ethanol. It was then, dried at 110°C and calcinated at 600°C.

*Present address: Département de Chimie Université Hassan II, Faculté des Sciences Aïn Chock, B.P. 5366 Maârif, Casablanca, Morocco.
**Present address: Département de Chimie Université Chouaîb Doukkali, Faculté des Sciences, Eljadida, Morocco.
†TZ3YB — Tosoh Corporation Japan.

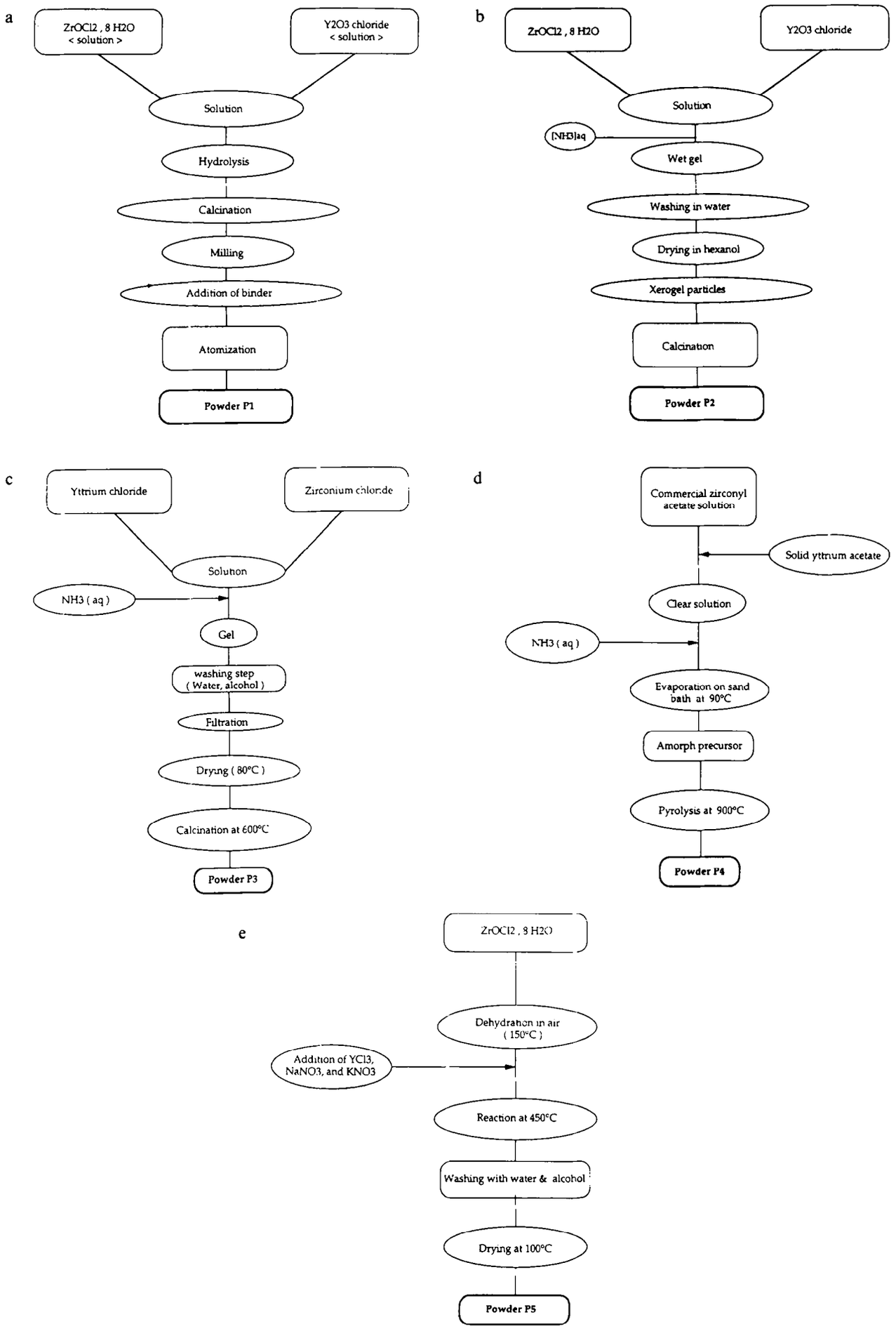

Fig. 1. Flowcharts of synthesis processes involved to prepare the five zirconia powders. (a) Synthesis process of the powder P1; (b) synthesis process of the powder P2; (c) synthesis process of the powder P3; (d) synthesis process of the powder P4; (e) synthesis process of the powder P5.

Table 1. Sample characteristics

Sample	*Synthesis route*	*Y_2O_3 (mol%)*	*Specific surface area (m^2/g)*	*Agglomerates mean size (μm)*	*Crystallite mean diameter (nm)*
P1	—	3	17	53·3	93
P2	Sol–Gel	3·6	100	34	9
P3	Sol–Gel	2	80	12·5	9
P4	Hydroxyacetate	3	6	100	25
P5	Molten salts	3	120	1·7	10

The powder, P4, was prepared from acetates. Solid yttrium acetate was dissolved in commercial zirconyl acetate solution. Then, the clear solution was neutralized by adding ammonia. The wet gel obtained was dried on a sand bath at 90°C and finally calcinated at 900°C in order to obtain white zirconia.

The powder, P5, was prepared by reacting both zirconia and yttria chlorides in molten salts at 450°C.

All the powders are yttrium stabilized zirconia, the amount of Y_2O_3 varying from 2·0 to 3·6 mol% (see Table 1).

The granulometric distribution of the different batches was obtained using a laser particle size analyser† and their morphology was investigated by scanning electron microscopy (SEM). The mean diameter of crystallites was determined from X-ray diffraction line broadening (XRD-LB) using the Scherrer formula for the calculation:

$$D = 0{\cdot}89\ \lambda/(\beta\ \mathrm{Cos}\theta)$$

where D is mean diameter of crystallites, λ the wave length of the X-ray (Cu–Kα), θ is the Bragg angle and β is the calibrated width of the diffraction peak at half maximum at selected 2θ. The proportion between the phases (monoclinic and tetragonal zirconia) was estimated using the empirical equation given by Toraya *et al.*[7] The specific surface area was evaluated by Brunauer–Emett–Teller (BET) nitrogen adsorption method.

Compaction tests were carried out on a mechanical testing machine‡ from 0 to 200 MPa with a crosshead rate of 0·5 mm/min so as to avoid the influence of loading rate.[8] In order to minimize the influence of moisture,[9,10] samples were oven dried at 110°C before compaction. Density variation during pressing was deduced from the crosshead continuous displacement. Deviation due to the elastic deformation of the die and the loading cell was taken into account with a blank test.

Porosity of the green samples was characterized by mercury penetration inside cold isostatic pressed pellets (400 MPa). The open porosity distribution could thus be quantified. Microstructure was also investigated by SEM.

The sintering schedule was optimized by performing dilatometric tests on samples isostatically pressed at 400 MPa; the temperature was raised up to 1500°C, at a rate of 1°C/min and samples were held at this temperature for 2 or 3 h. The porosity and microstructure of sintered samples were also examined.

Results and discussion

The sample characteristics are shown in Table 1. From these results it is shown that:

- Powders P2 and P3, (sol-gel) and P5, (molten salt) exhibit much higher surface areas than powders P1, (commercial) and P4, (hydroxyacetate).
- The crystallite mean diameter of the commercial powder, P1 is consequently larger than that of the other powders.

The X-ray patterns of these powders (Fig. 2) indicates that powders P2, P3, P4 and P5 are fully

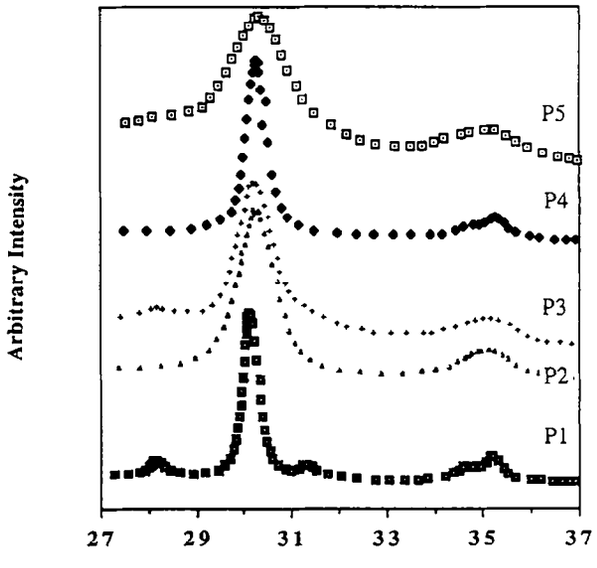

Fig. 2. X-ray patterns of the powders.

†Malvern particle size analyser 2000/3000.
‡Instron Ltd 1195.

stabilized into the tetragonal phase whereas the commercial powder, P1, contains a very low amount of monoclinic zirconia, about 3 vol%.

The SEM micrographs (Fig. 3) can divide the samples into three groups according to the shapes of the agglomerates: spheroidal (P1, P2 and P3), rod-like (P5) and irregular (P4).

The compaction plots (Fig. 4) of all the powders, density versus applied pressure, shows two linear regions separated by a transition zone. The first linear region, localized at low pressures and characterized by a low slope, is consistent with a rearrangement of the agglomerates in the die. This stage is controlled by particle–particle friction,

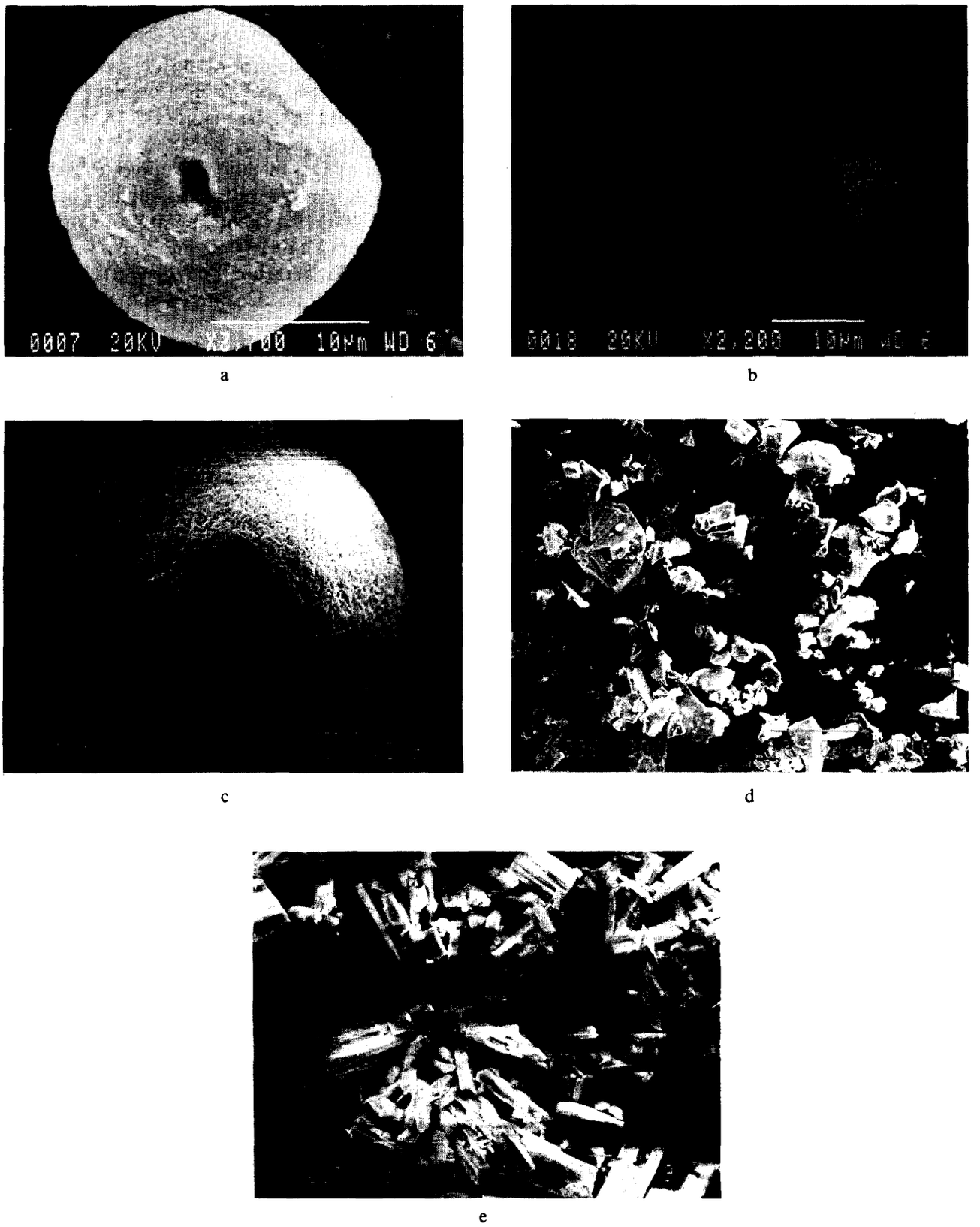

Fig. 3. Scanning electron micrographs of loose powders. (a) powder P1; (b) powder P2; (c) powder P3; (d) powder P4; (e) powder P5.

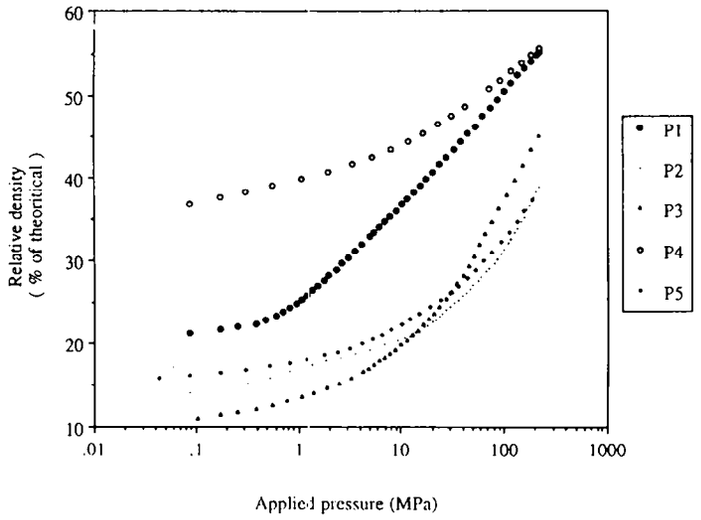

Fig. 4. Compaction behaviour of the five zirconia batches.

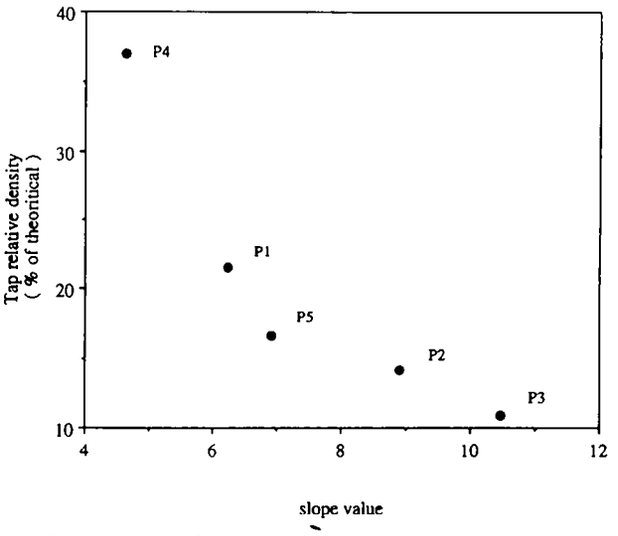

Fig. 5. Plot showing the compaction slope versus tap density. The slope was calculated for each powder in high pressure linear region according to Zheng.

Table 2. Compaction characteristics of the samples

Sample	*P1*	*P2*	*P3*	*P4*	*P5*
Tap density	21·45	14·16	10·83	37·08	16·66
Slope value	6·23	8·90	10·46	4·62	6·90
Pj (MPa)	1	30	11	11	15

until they are on fixed positions to each other.[7,11] The second linear region occurs at higher pressure having a more significant slope, corresponds to the elimination of the interagglomerate porosity.[7,11] The transition zone exhibits a particular pressure value *Pj* for each powder, known as the 'yield point.'[7,11,12] This threshold pressure corresponds to the beginning of the agglomerate deformation and/or crushing. It indicates a transition from discrete agglomerate structure to a coherent compact structure. Compared to the commercial powder, P1, the tap density of powder P4 is about 50% higher whereas for powders P2, P3 and P5 it is lower. For powder P4, even if the shape of agglomerates is irregular, their high density and large size (100 μm) allows this high tap density. For P1 powder, exhibiting the same shape of agglomerates as for the powders P2 and P3, the high tap density is favoured by the large size (53·3 μm) and density of agglomerates. This later allows easy rearrangement in the die. On the contrary, the small size of P2 and P3 agglomerates (mean size 34 and 12·5 μm respectively) and also their porous morphology in the case of the powder P3 favours low tap density. For the powder P5, the rod-like shape of agglomerates involves a bad flowability and consequently a weak green density.

The slopes of the curves in the high pressure linear region have been calculated (Table 2), and plotted versus taped densities (Fig. 5) in the same

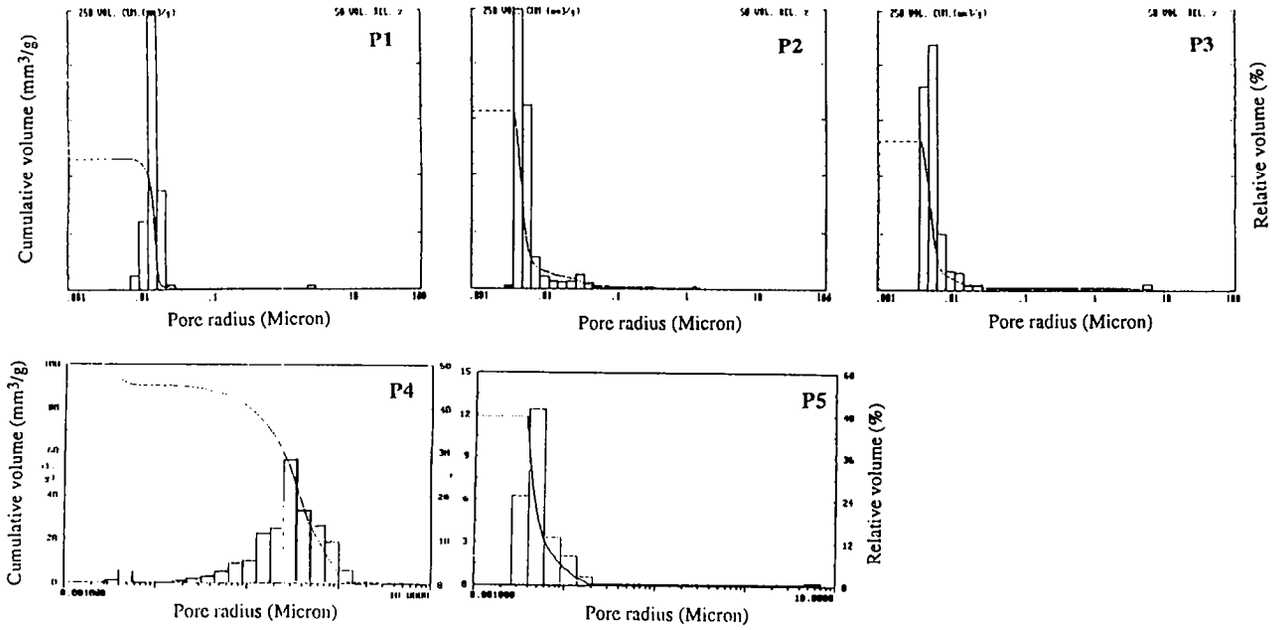

Fig. 6. Pore size frequency distribution in dry isostatically pressed compacts (400 MPa).

way as Zheng and Reed.[13] The compaction rate varies inversely to the powder tap density. The more the powder is constituted of large and dense agglomerates, the more the agglomerates are difficult to deform and/or to crush.

For the powder P1, the yield pressure is about 1 MPa, whereas for the laboratory prepared powders, P2, P3, P4 and P5 it is close to 10 MPa. The difference could be explained by the presence of a binder/plasticizer system in powder P1, allowing

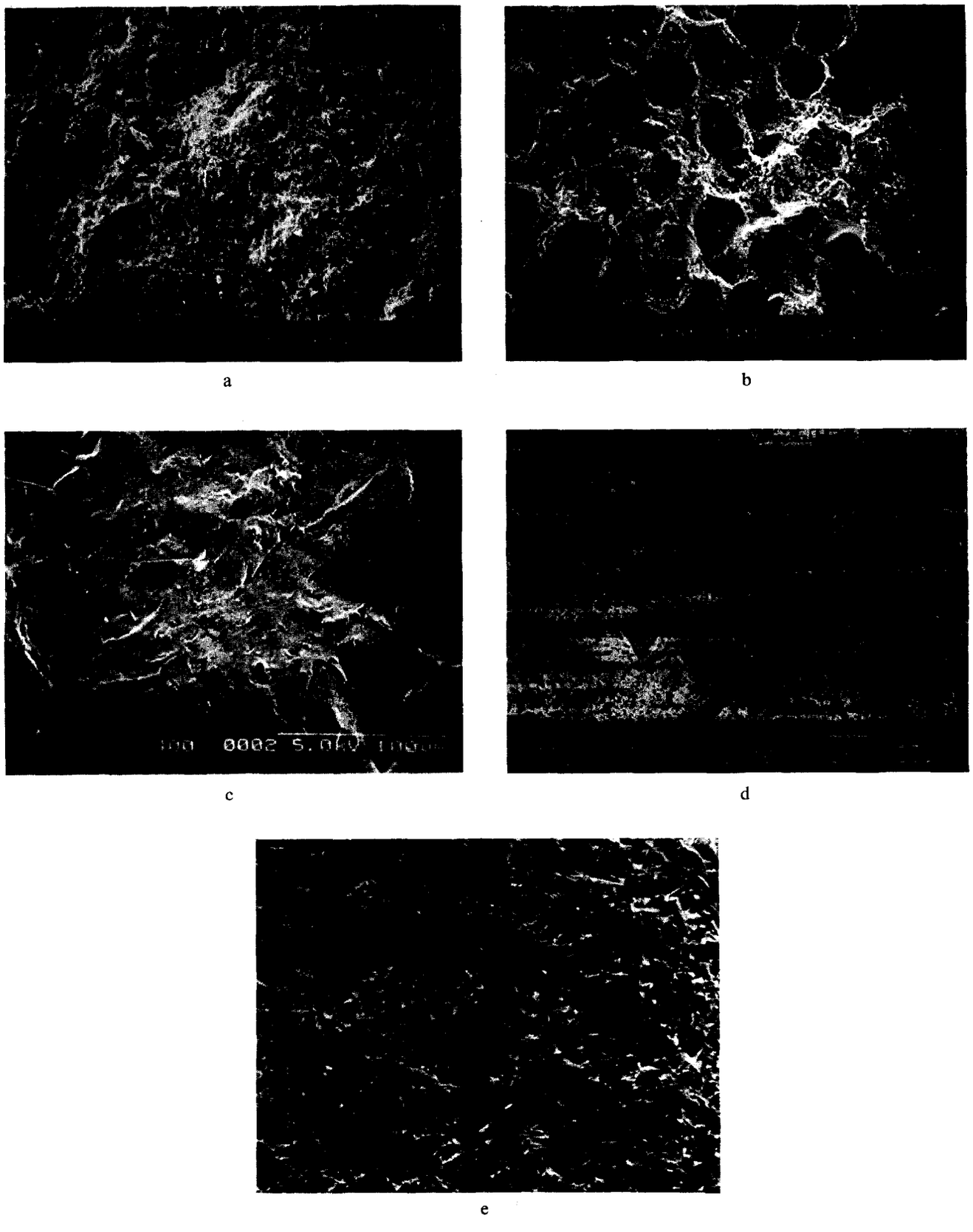

Fig. 7. Series of scanning electron micrographs showing fractured surfaces of green bodies isostatically compacted up to 400 MPa. (a) Fractured surface of green compacted P1; (b) fractured surface of green compacted P2; (c) fractured surface of green compacted P3; (d) fractured surface of green compacted P4; (e) fractured surface of green compacted P5..

easy plastic deformation of agglomerates at low applied pressure. Then, they crush easily and the particles slide onto each other, favouring inter and intra-agglomerate porosity elimination and thus better compaction.

Mercury porosimetry data (Fig. 6) shows a pore distribution radii in the range 0·01–10 μm for all samples isostatically compacted at 400 MPa. The maximum porous volume is localised in the low value side for P1, P2, P3 and P5 (near 0·01 μm) and at the larger side value for P4 (near 0·7 μm). If the pore mean diameter of each powder is compared to crystallite mean diameter obtained from X-ray patterns, we can easily notice that the samples P1, P2, P3 and P5 exhibit mainly intercrystallite porosity. In addition, a very small interaggregate porosity is noticed for samples P2 and P3 with pore radii more than 0·01 μm. On the contrary, the sample P4 exhibits essentially large interaggregate pores. Very weak intercrystallite porosity is also seen at about 5 nm. So, this powder is essentially formed of dense aggregates.

The SEM characterization of green bodies (Fig. 7) shows that:

- The compaction process of powders P1, P3 and P4, at pressures higher than *Pj*, is controlled by a crushing phenomenon of their agglomerates.
- For powder P5, it is also controlled by the crushing of agglomerates but some rod-like shaped agglomerates remain after pressing.
- For powder P2, the integrity of agglomerates is conserved even after pressing up to 400 MPa. Consequently large pores are still present in the green bodies.

The shrinkage of P2, P3 and P5, characterized by a high specific surface area (close to 100 m^2/g),

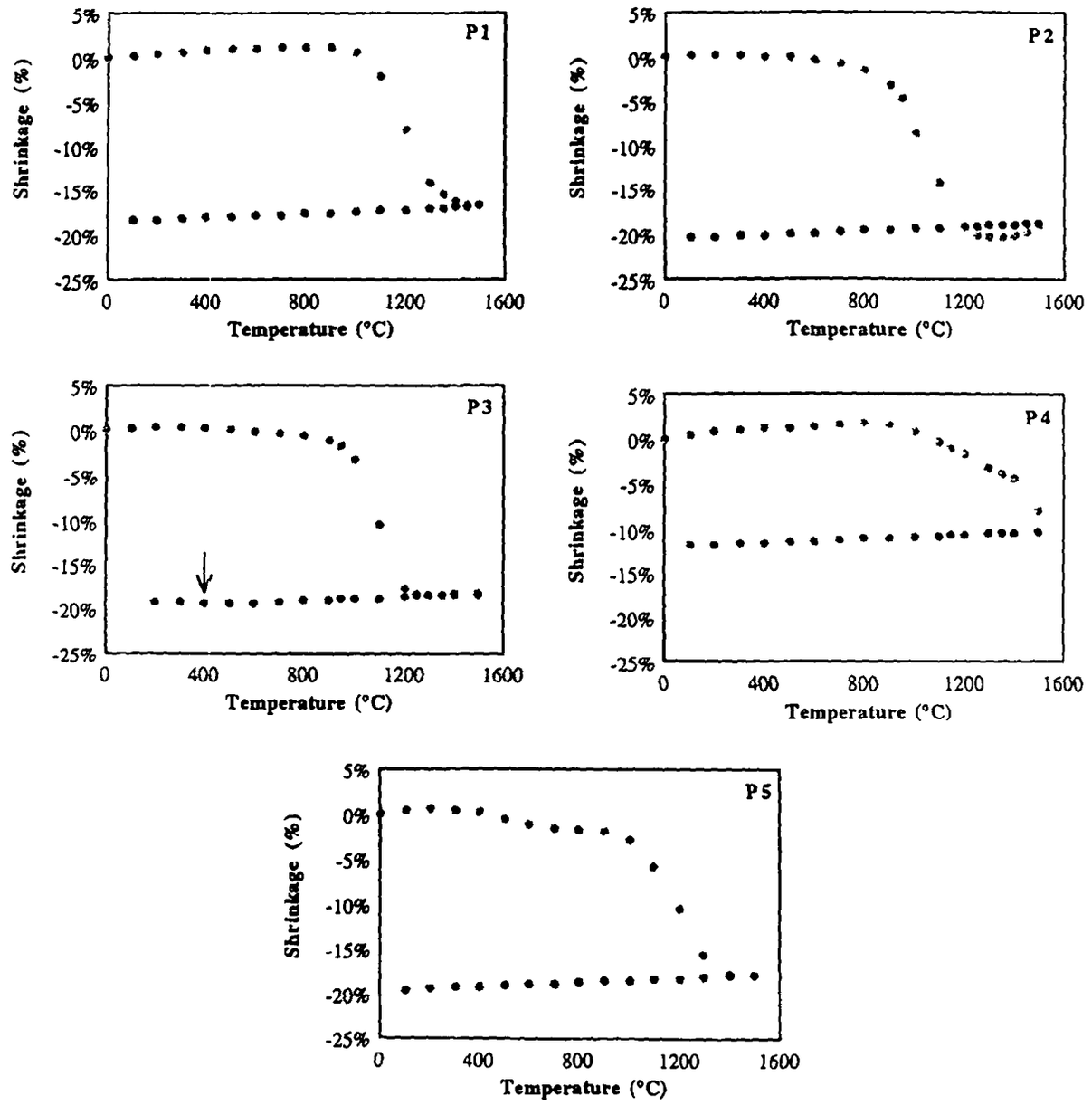

Fig. 8. Dilatometric curves of samples isostatically packed up to 400 MPa and sintered up to 1500°C with a heating rate of 1°C/min.

starts at 400°C and reaches about 20%. Shrinkage is also significant for the powder P1 but begins only at 850°C. Powder P4 has the lowest surface area and shrinkage starts at 850°C and does not exceed 12%, (Fig. 8). Thus, the reactivity of the powders P2, P3 and P5 allows a good densification during the sintering stage, though they have a low green density. The sintering stage of powder P4 is largely delayed by the presence of a large porosity, which is difficult to eliminate at 1500°C

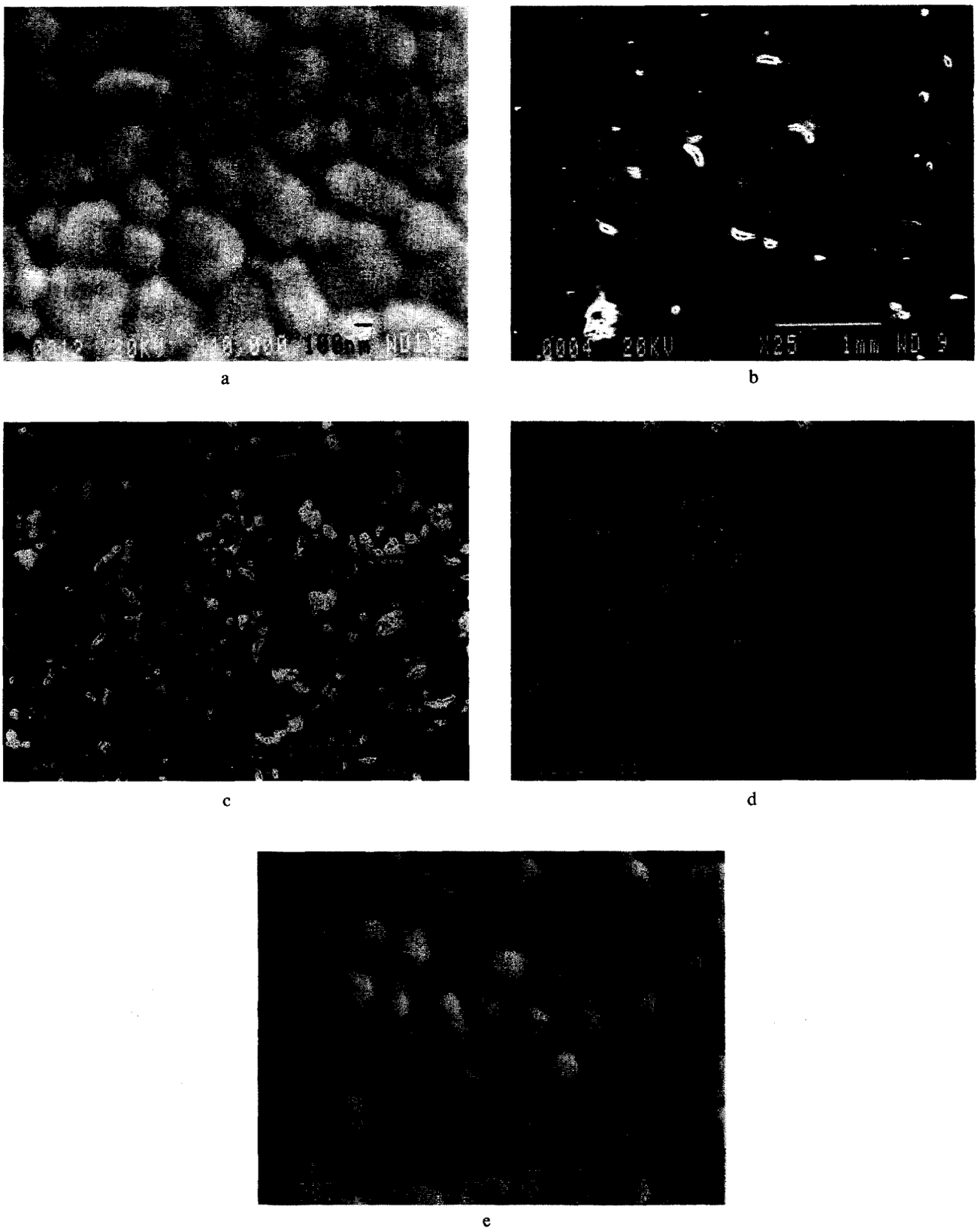

Fig. 9. Series of scanning electron micrographs of sintered (1500°C) pellets made from the powders compacted up to 400 MPa. (a) Micrograph of sintered P1 sample; (b) micrograph of sintered P2 sample; (c) micrograph of sintered P3 sample; (d) micrograph of sintered P4 sample; (e) micrograph of sintered P5 sample.

Table 3. Density of green and sintered samples, % of theoretical

Sample		*P1*	*P2*	*P3*	*P4*	*P5*
Green		54·67	46·78	49·09	58·52	52·17
Sintered	1350°C	—	96·16	94·09	—	—
	1500°C	99·83	88·44	91·99	79·01	98·7

probably owing to the hardness of agglomerates which have not been crushed during pressing. Dilatometric curves of sol–gel powders P3 and principally P2 show a dedensification above 1350°C as previously observed in earlier work.[14,15]

Dilatometric data are confirmed by the measurement of the density of sintered pellets using Arthur's method[16] (Table 3). A density close to 95% of theoretical is reached for samples P2 and P3 sintered at 1350°C. The marked density decrease for the pellets sintered at 1500°C can be explained both by the opening of large pores and the presence of microcracks as shown in SEM micrographs (Fig. 9). Microcracks seen on the micrograph of sample P3, are induced by an increase in monoclinic zirconia content due to grain growth which causes lower density. The tetragonal to monoclinic transformation occurs during the cooling stage as is evident from a dedensification mentioned by the arrow on the dilatometric curve, (Fig. 8) and the presence of monoclinic zirconia on XRD patterns, (Figs 10 and 11).

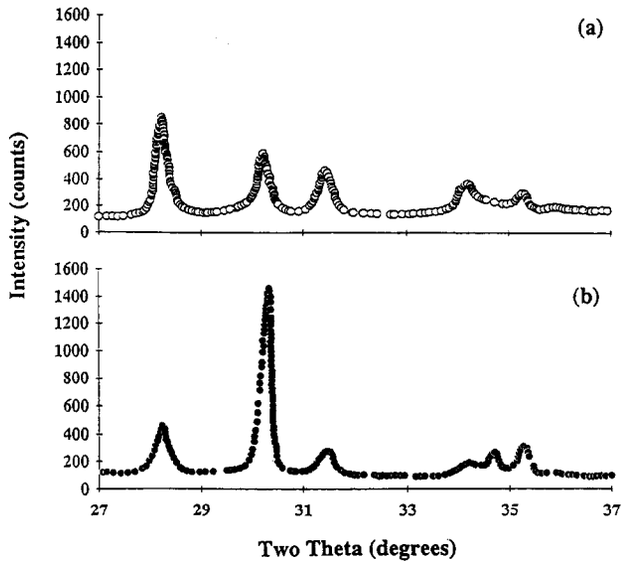

Fig. 11. XRD patterns of P3 sintered (a) at 1500°C, (b) at 1350°C pellets.

The pattern of the other sintered samples indicates only the presence of tetragonal zirconia (Fig. 10). This difference of behaviour is interpreted as a consequence of a lower amount of Y_2O_3 in sample P3. The dedensification phenomenon of sample P2 is a consequence of differential sintering leading to circumferential cracks around hard granules.[17]

A density close to 99 and 98% of theoretical is reached respectively for samples P1 and P5 exhibiting a regular microstructure. The SEM micrograph of sample P4 shows a large porosity which can not be eliminated below 1500°C. TGA experiments (Fig. 12) coupled with gas release

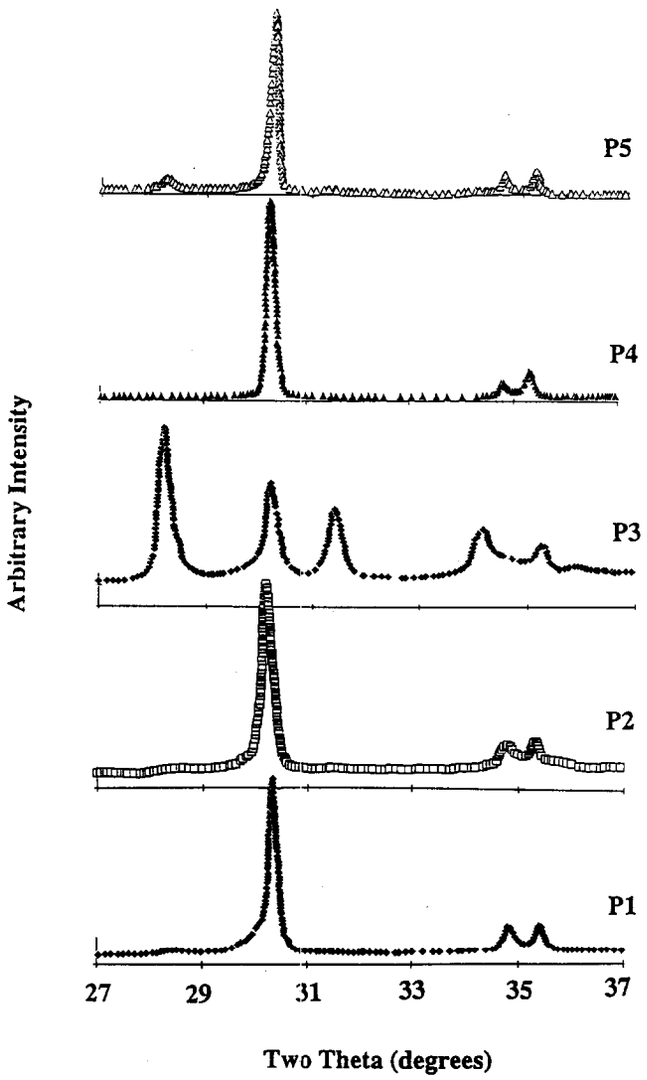

Fig. 10. XRD patterns of compacts sintered at 1500°C.

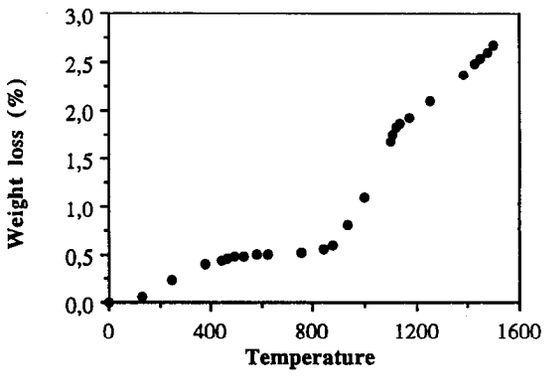

Fig. 12. Thermogravimetric data (TGA) of the sample P4 isostatically packed (400 MPa).

analysis show that the decomposition of residual carbon may be in the form of carbonate or oxycarbonate groups beginning beyond 900°C and not finished at 1500°C. So, a density of 78% of theoretical isn't exceeded.

Conclusions

The commercial powder has a higher mean crystallite size, it sinters quite well and a regular microstructure is obtained. This is due to plastic behaviour of the granules during the compaction stage. The binder favours compaction and allows an earlier crushing of the agglomerates at very low applied pressures. Then, narrower porosity distribution in the green samples leads to good densification.

The reactivity and the fine grain size of sol–gel powders allows a very low sintering temperature. The granulation process involves very good flowability, but it must be controlled carefully to avoid the formation of hard agglomerates. This could be achieved by lowering the calcination temperature down to 400–500 as proposed by Van de Graaf *et al.*[15]

The presence of residual carbon in the form of carbonate or oxycarbonate groups in the sample P4 inhibits the sintering of this powder. Their decomposition begins beyond 900°C and is not finished at 1500°C. Also the presence of aggregates is the second major inconvenience which inhibits the sintering stage.

The molten salt route is interesting because sintered bodies reach the theoretical density. The morphology of this powder must be optimized by changing synthesis parameters so as to enhance flowability.

Acknowledgements

The authors wish to thank Prof. A. Negro, Dr B. Guilhot, Dr J. Dubois, Dr L. Montanaro and Dr J. M. Missiaen for their collaboration and fruitful discussions.

References

1. Dynys, F. W. & Halloran, J. W., Influence of aggregates on sintering. *J. Am. Ceram. Soc.*, **67**(9) (1984) 596–601.
2. Pampuch, R. & Haberko, K., Agglomerates in ceramic micropowders and their behaviour on cold pressing and sintering. In *Ceramic Powders*, Ed by P. Vincenzini. Elsevier Science Ltd, Amsterdam, 1983, pp. 623–34.
3. Ciftcioglu, M., Akinc, M. & Burkhart, L., Effect of agglomerate strength on sintered density for yttria powders containing agglomerates of monosize spheres. *J. Am. Ceram. Soc.*, **70**(11) (1987) C329–34.
4. Montanaro, L., Elaboration des poudres céramiques par voie sol-gel: application aux dispersoïdes alumine-zircone et à la zircone yttriée, PhD thesis, I.N.P.G.-E.N.S.M. de St Etienne, (1990).
5. Samdi, A., Grollier-Baron, T., Durand, B. & Roubin, M., Préparation par hydrolyse de solutions aqueuses, d'acétates de zirconium et d'yttrium précurceurs de zircones dopées à l'yttrium finement divisées, *Ann. Chim., Fr.*, **13** (1988), 517–26.
6. Jebrouni, M., Durand, B. & Roubin, M., Elaboration de zircone pure par réaction en milieu nitrate fondu et caractérisation, *Ann. Chim., Fr.*, **16** (1990) 569–79.
7. Toraya, H., Yoshimura, M. & Somiya, S., Calibration curve for quantitative analysis of the monoclinic–tetragonal ZrO2 system by X-ray diffraction. *J. Am. Ceram. Soc.*, **75**(4) (1984) C119–21.
8. Matsomoto, R. L. K., Analysis of powder compaction using compaction rate diagram. *J. Am. Ceram. Soc.*, **73**(2) (1990) 465–8.
9. Dimilia, R. A. & Reed, J. S., Dependence of compaction on glass transition temperature of the binder phase. *Ceram. Bull.*, **62**(4) (1983) 484–8.
10. Frey, R. G. & Halloran, J. W., Compaction behavior of spray-dried Alumina. *J. Am. Ceram. Soc.*, **67**(3) (1984) 199–203.
11. Holman, L. E., The compaction behaviour of particulate materials. An elucidation based on percolation theory. *Powder Technol.*, **66** (1991) 265–80.
12. Messing, G. L., Markhoff, C. J. & McCoy, L. G., Characterization of ceramic powder compaction. *Ceram. Bull.*, **61**(8) (1982) 857–60.
13. Zheng, J. & Reed, J. S., Particle and granule parameters affecting compaction efficiency in dry pressing. *J. Am. Ceram. Soc.*, **71**(11) (1988) C456–8.
14. Smith, A., Baumard, J. F., Sinterability of tetragonal ZrO2 powders. *Am. Ceram. Soc. Bull.*, **66**(7) (1987) 1114–8.
15. Van de Graaf, M. A. C. G., Ter Maat, J. H. H. & Burggraaf, A. J., Microstructural development during pressing and sintering of ultra fine zirconia powders. In *Ceramic Powders*, ed P. Vincenzini. Elsevier Science Ltd, Amsterdam, 1983 783–94.
16. Arthur, G., Porosity and permeability change during the sintering of copper powder. *J. Inst. Met.*, no. **83**, 1954–5, pp. 329–36.
17. Jorand, Y., Taha, M., Missiaen, J. M. & Montanaro, L., Compaction and sintering behaviour of sol-gel powders. submitted to *J. Euro. Ceram. Soc.*